Journal of Environmental Monitoring

Dynamic Article Links

Cite this: *J. Environ. Monit.*, 2011, **13**, 3460

www.rsc.org/jem

PAPER

Mercury emission and dispersion models from soils contaminated by cinnabar mining and metallurgy

Willians Llanos,[ab] David Kocman,[c] Pablo Higueras[a] and Milena Horvat[c]

Received 26th August 2011, Accepted 27th September 2011
DOI: 10.1039/c1em10694e

The laboratory flux measurement system (LFMS) and dispersion models were used to investigate the kinetics of mercury emission flux (MEF) from contaminated soils. Representative soil samples with respect to total Hg concentration (26–9770 μg g^{-1}) surrounding a decommissioned mercury-mining area (Las Cuevas Mine), and a former mercury smelter (Cerco Metalúrgico de Almadenejos), in the Almadén mercury mining district (South Central Spain), were collected. Altogether, 14 samples were analyzed to determine the variation in mercury emission flux (MEF) *versus* distance from the sources, regulating two major environmental parameters comprising soil temperature and solar radiation. In addition, the fraction of the water-soluble mercury in these samples was determined in order to assess how MEF from soil is related to the mercury in the aqueous soil phase. Measured MEFs ranged from less than 140 to over 10 000 ng m^{-2} h^{-1}, with the highest emissions from contaminated soils adjacent to point sources. A significant decrease of MEF was then observed with increasing distance from these sites. Strong positive effects of both temperature and solar radiation on MEF was observed. Moreover, MEF was found to occur more easily in soils with higher proportions of soluble mercury compared to soils where cinnabar prevails. Based on the calculated Hg emission rates and with the support of geographical information system (GIS) tools and ISC AERMOD software, dispersion models for atmospheric mercury were implemented. In this way, the gaseous mercury plume generated by the soil-originated emissions at different seasons was modeled. Modeling efforts revealed that much higher emissions and larger mercury plumes are generated in dry and warm periods (summer), while the plume is smaller and associated with lower concentrations of atmospheric mercury during colder periods with higher wind activity (fall). Based on the calculated emissions and the model implementation, yearly emissions from the "Cerco Metalúrgico de Almadenejos" decommissioned metallurgical precinct were estimated at 16.4 kg Hg y^{-1}, with significant differences between seasons.

1. Introduction

Due to its volatile nature, mercury (Hg) emission from terrestrial and aquatic surfaces is an important part of its biogeochemical cycle.[1] Recent assessment on the global scale showed that the contribution from anthropogenic sources in 2005 ranges between 1926 and 2320 Mg y^{-1},[2,3] whereas emissions from natural sources (*i.e.*, volatilization from water surfaces, volcanoes, re-emissions from topsoil and vegetation) may represent the major

[a]*Instituto de Geología Aplicada, Universidad de Castilla-La Mancha, EIMI Almadén, Pl. Manuel Meca, 1, 13400 Almadén, Ciudad Real, Spain*
[b]*Departamento de Cristalografía y Mineralogía, Universidad Complutense de Madrid, Av. Complutense s/n., 28071 Madrid, Spain*
[c]*Department of Environmental Sciences, Jožef Stefan Institute, Ljubljana, Slovenia*

Environmental impact

Gaseous mercury emission from contaminated soils represents an important contribution to the presence of this pollutant in the atmosphere, and it depends on the mercury concentration and speciation in the soil, and also on meteorological variables such as temperature and sun radiation. Experimental work aimed to study in detail variability caused by these parameters has been carried out and has successfully allowed the modeling of mercury distribution plumes around these sources, as well as to quantify the net mercury output coming from a contaminated area. The study has been carried out in the world's largest mercury mining area: Almadén district (Spain).

contribution (up to 5200 Mg y^{-1}) to the global atmospheric mercury budget.[3] Contaminated sites such as abandoned Hg mining areas and surrounding geologically enriched terrains are known atmospheric mercury sources.[4] Mercury emission rates from these Hg-enriched areas were found to be greater than previously estimated, indicating that these sources may be more significant contributors of mercury to the atmosphere than previously realized.[5–8] Moreover, it is known that mercury emitted from such contaminated sites can be deposited locally or transported over long distances and deposited even at the most remote sites far from direct discharges of mercury.[9] However, information on emission rates, their spatial extent, as well as parameters influencing the emission processes at these sites is relatively scarce.

Here, we investigated site-specific factors controlling mercury release and dispersion from contaminated soils in the Almaden mercury mining district, Spain. Almadén (Ciudad Real province, South Central Spain) is the largest mercury mining district in the world, with a total production of around 300 000 tones of liquid metal—around one-third of the total mercury produced historically.[10] Today Almadén is faced with a number of polluted sites, and contaminated soil spread around the area. In the soils from the Almadén district most of the mercury pollution comes from mining, and so it is in the form of cinnabar,[11–13] a very stable mineral phase relatively unavailable for transformation into volatile mercury species.[1] However, physicochemical and biological reactions, in part photocatalyzed, allow the formation of more labile phases, allowing the emission of metal vapors. For practical purposes, the fact is that mercury-containing soils are major emitters of mercury vapors. In this study, soil samples surrounding a decommissioned mercury-mining area (Las Cuevas Mine) and a former mercury smelter (Cerco Metalúrgico de Almadenejos) were analyzed to determine the variation in mercury emission flux (MEF) *versus* distance from the sources, regulating two major environmental parameters comprising soil temperature and solar radiation. The fraction of the water-soluble mercury in these samples was also determined in order to assess how MEF from soil is related to the mercury in the aqueous soil phase. In addition, based on the measured mercury emission rates, dispersion models for atmospheric mercury were implemented to generate the mercury plume by the soil-originated emissions at different seasons.

2. Materials and methods

2.1. Field sites

For this study we have considered two different areas:

(A) Cerco Metalúrgico de Almadenejos (CMA): It corresponds to a decommissioned metallurgical precinct, enclosed by a 3 m high wall, located some 13 km to the ESE from Almadén and immediately to the North from the village of Almadenejos. Martínez-Coronado *et al.*[14] describe in detail this area, as well as the soil sampling survey carried out in this area.

(B) Las Cuevas Mine (LCM): It corresponds to a mine area, in activity from 1983 to 2000;[15] since 2004 it is the mercury handling and storage facility belonging to MAYASA, the local mining company. It is located some 10 km to the northeast of Almadén, in proximity to the CN 415 road. Llanos *et al.*[16] describe in detail this area and make an estimation of emissions coming from the mercury handling facility.

We have studied a total of seventy five samples, corresponding to samples used in the above mentioned previous studies (Llanos *et al.*[16] and Martínez-Coronado *et al.*[14]), and were selected on the basis of total mercury content variability. Fig. 1 shows the location of the samples in their regional contexts.

2.2. Sample characteristics

One of the objectives of this study was to determine the emission mercury flux from local soils to the atmosphere. However, these determinations cannot be carried out without the prior control of the edaphic factors involved in the volatilization of the element. In this sense, the chosen methodology is based on the technique proposed by Walkley and Black,[17] for determination of active organic carbon, and converted to organic matter content by multiplying by the Van Bemmelen factor of 1.724.[18] It is based on the oxidation of organic matter with a mixture of potassium dichromate and sulfuric acid. The residual dichromate is valued with a ferrous sulfate solution.

The pH and EC (electric conductivity) of the samples are measured with a potentiometer (pH-meter CRISON GLP 22) and a conductivimeter (CRISON GLP 32) in a suspension of soil–liquid mixture (1 : 2.5). The liquid is Milli-Q water (pH—H_2O). On the other hand the soil texture was established by means of the Boyuocos method, based on the sedimentation speed (Stokes law).

2.3. Determination of total mercury

The analysis of soil samples for total mercury was carried out at room temperature in dry samples, disintegrated and split to extract an aliquot; this aliquot is ground to less than 100 μm size with an agate mortar. From these samples we extract 5–10 mg, which is used for analysis. Three analyses (replicates) were performed by sample, by means of a LUMEX RA-915+ equipment, based on Zeeman atomic absorption spectrometry, with high frequency modulation of light polarization (ZAAS-HFM).[19]

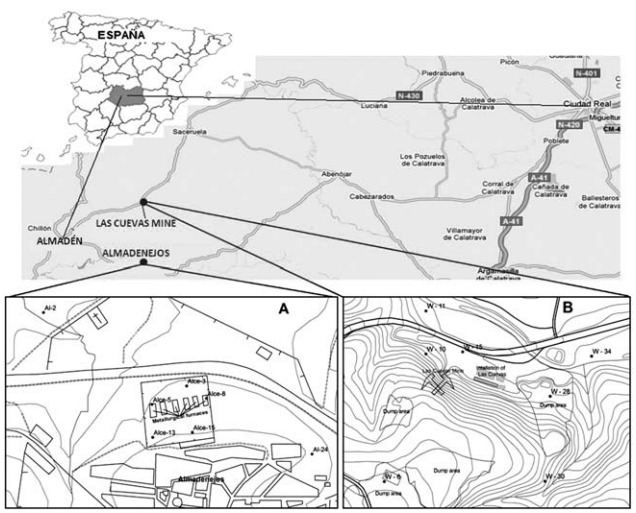

Fig. 1 Study area and sample location in the CMA (A) and LCM (B) areas.

Application of the Zeeman background correction and a multi-path analytical cell provide high selectivity and sensitivity of measurements. Addition of the RP-91C (pyrolysis) attachments allows Hg measurements in the soil samples: mercury in the samples is converted from a bound state to the atomic state by thermal decomposition in a two-section atomizer. As a first step the sample is vaporized and the mercury compounds are partly decomposed. This is followed by heating to 800 °C, when the mercury compounds become fully decomposed, whereas organic compounds and carbon particles are catalytically transformed to carbon dioxide and water. Using Zeeman correction for non-selective absorption eliminates all interference as dust, aerosols and other absorbing gases. The analysis takes 1–2 min, and the detection limit for total Hg is 0.5 μg kg^{-1}. For the analysis of samples with extremely high mercury content, the equipment has an auxiliary compartment, allowing incorporation of an additional analytic cell that increases the measurement range.

Quality control is accomplished by analyzing replicate samples to check precision, whereas accuracy was obtained by using certified standards: (SRM) NIST 2710, (SRM) NIST 2711, and BCR 146R. As a first step, the measuring equipment was calibrated using SRM reference standards (NIST 2710 and 2711) in total mercury content (32.600 and 6.250 ng g^{-1} respectively), which were also used periodically to check the measuring equipment during the analyses to avoid deviations.

2.4. Water-soluble mercury fraction

Water soluble mercury fractions were extracted using the first step of the sequential extraction procedure proposed by Bloom *et al.*[20] 30 mL of rain water were added to 0.5 to 1 g of solid contained in glass vials of 50 ml and shaken end-over-end at 250 rpm for 18 h. The vials were then centrifuged at 3800 rpm for 10 min, and the supernatant liquid was filtered through a membrane filter of 0.45 μm pore size, these filters were used only once and then discarded. These are disposable syringe filters, used in our and other labs for separation of the operationally defined dissolved and particulate Hg phases. Therefore, these filters were rigorously tested before and are not Hg contaminated. The filtrate was deposited in a 50 ml glass vial, and was then oxidized using BrCl 0.2 M (0.4 ml) and HCl (0.2 ml). Total Hg in the oxidized fraction extract was determined using 10–11 ml of $SnCl_2$ reduction agent, together with 10–15 ml of Milli-Q water; Hg^0 was measured with a SANSO SEISHA-KUSHO CV AAS Hg analyzer, Instrument Model 910, Japan. Quality control included reagent blanks to assess contamination. The reagents have a high quality, and they are the same reagents used by the accredited laboratory of Jožef Stefan Institute (Ljubljana, Slovenia) in the determination of mercury in sediments and soils.

2.5. Laboratory flux measurement system (LFMS)

Mercury emissions from soil samples were determined using the flux chamber technique.[21–24] Two different sized chambers, C_1 and C_2, were used, both made of 5 mm thick Plexiglas and with a semi-cubic form, but of different dimensions (C_1: small chamber and C_2: large chamber) with areas of 195.99 and 612.56 cm^2, with heights of 9.5 cm (C_1) and 20 cm (C_2) (Fig. 2).

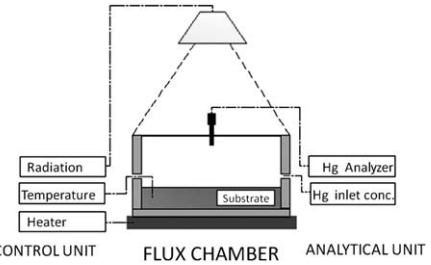

Fig. 2 Experimental setup of the laboratory chambers.

The smaller chamber (C_1) was used, together with the measuring instrument UTM 3000, for measuring lower Hg concentrations (0–1000 ng m^{-3}). The large chamber (C_2) was used with the mercury analyzer LUMEX RA-915+ for measurements of samples with higher Hg concentrations (1000–10 000 ng m^{-3}). Temperature was varied by means of a Tehtnica Rotamix-SHP-10 heating block and measured with a resistance temperature detector.

Experiments conducted as a function of light intensity were carried out mostly under room conditions, some of them using an ultraviolet lamp with a constant intensity of 32.6 Klx (273 W m^{-2}). At the first stage, samples were subject to temperature increases from 20 to 50 °C with increments of 5 °C over time spans between 5 and 60 min under constant radiation (300–350 lux) coming from artificial lighting provided by the laboratory (dark conditions). At the second stage the samples were subjected to higher intensity light radiation provided by the ultraviolet lamp which produced an increase of sample temperature from 20 to 35 °C during time spans between 40 and 120 min. At the third stage, lighting was reverted to dark conditions and kept in these conditions during time spans between 45 min and 3 hours. In all cases, mercury emission was measured in the chamber until its rate stabilized, explaining the time differences between samples.

The Mercury Emission Flux (MEF) was determined from the formula (1):[24–26]

$$\mathrm{MEF} = \frac{\Delta C Q}{A} \quad (1)$$

where MEF is the Mercury Emission Flux (ng m^{-2} h^{-1}), $\Delta C = C_1 - C_0$ (emission concentration gradient) in ng m^3, Q is the flow rate (m^3 h), and A is the chamber surface (m^2).

Mercury emissions were monitored using two instruments. In the UT-3000 the gas sample passes first through a 0.45 μm filter, then through a gold trap, capturing any mercury. The gold trap is then heated rapidly, releasing the mercury as vapor. This gaseous mercury is swept by mercury-free air into the optical cell detector, to be quantified by means of atomic absorption. The LUMEX RA-915+ is able to analyze gaseous mercury at time intervals dictated by the operator. The analysis is carried out in a forced air flow of 12 l min^{-1}, passing through the atomic absorption cell, which quantifies the concentration of mercury present in the air flow, with a detection limit of 2 ng Hg m^{-3} and a measurement range up to 20 000 ng Hg m^{-3}.

2.6. Modeling of mercury plumes

This study is aimed at the implementation of gaseous mercury dispersion models, constrained with data from *in situ*

measurements of gaseous mercury concentrations, to provide a realistic characterization of emission processes and sources responsible of the presence of mercury in the atmosphere. It is based exclusively in the CMA area and, for the model implementation, we have used Lakes Environmental ISC-AERMOD program developed by the U.S. Environmental Protection Agency (http://www.air-dispersion-model.com/html/air-quality.html). This is a complete and powerful package that models dispersion of pollutants in the air, and incorporates in a single interface three subprograms: ISCST3, ISC-PRIME and AERMOD. The program uses a Gaussian distribution for modeling (ISCST3), algorithm integrators (ISC-PRIME) and a regulator of plume system modeling (AERMOD). Additionally, the software has an applet (AERMET View) that incorporates topographical features as well as land uses. For modeling we used meteorological data for the year 2009, divided into seasonal periods of spring, summer and fall. Modeling for the winter season was not carried out due to the low temperatures reached by the soil during this season, making it unfeasible to represent these environmental conditions in the laboratory.

On the other hand the measurement of gaseous mercury concentration was performed in different field surveys in the same time period as the modeling (2009). This part of the study was complemented by local monitoring of meteorological variables by means of a meteorological station brand DAVIS model Vantage Pro2, consisting of a control unit plus a measuring unit connected by radio frequency. The station collects and stores data every 15 minutes for the following parameters: temperature (°C), environment humidity (%), barometric pressure (mm), dew point, wind direction in degrees, wind speed (m s^{-1}), solar radiation (W m^{-2}), rainfall (l m^{-2}), and soil temperature and moisture. We used a single year (2009) for theoretical modeling in order to contrast the data measured in the field during this year with results from the theoretical model.

3. Results and discussion

3.1. Sample edaphic characteristics and total mercury

As mentioned above, in order to characterize the mercury emission flux from soil, we have also characterized the edaphic factors involved in the volatilization of the element, as well as the soil mercury contents (Table 1). pH for LCM area soils is slightly acid in a range between 5 and 6, while the CMA area has values slightly alkaline (8–9). According to this relation we can deduce that local characteristics for LCM area soils favor the release of mercury, meanwhile in the CMA area the pH levels are a limiting factor for availability of metal.[27] On the other hand, the EC values are between 73 and 373, and between 132 and 325 μS cm^{-1}, respectively for LCM and CMA areas, the samples with higher EC probably reflecting the formation of sulfate salts that minimize mercury mobility though the formation of schuetteite ($Hg_3(SO_4)O_2$), as confirmed by samples W-28 and Al-2, with the lowest EC values (73 and 182 μS cm^{-1} respectively) and producing considerable Hg emissions (Table 1).

The OM concentration has values between 1 and 4% (LCM) and 2–6% (CMA). Minimum OM concentrations are 1% in LCM sector (sample W-28), and 1.7–2.7% for the CMA area (samples: Al-2, Alce-8, Alce-5); this certainly could have affected the Hg emissions, as Wallschläger *et al.*[28] deduced that humic substances and the presence of Cd^{2+} enhance the abiotic reduction of Hg^{2+} to Hg^0. Meanwhile, the low proportions of clay in soils (6–20%) in the two studied areas should not affect mercury emissions; however the sample Al-2 has a considerable amount of clay (32%); a tentative interpretation of these data is that the drying of the sample during the thermal process used in the experiments implies the breakdown of the soil texture, favoring the emission process. In samples from the LCM area, mercury contents increase according to proximity to the local emission sources, with values over 1000 mg kg^{-1} at the minimum distances to less than 100 mg kg^{-1} at more than 350 m from the source. The same applies to CMA samples with reference to distance to the old metallurgical furnaces which act as active emission sources.[14] The highest Hg contents, more than 10 000 mg kg^{-1}, are found in samples Alce-8 and Alce-5, located on the furnace ruins, while, away from the furnaces and outside the precinct (samples AL-2 and 24), contents were less than 200 mg kg^{-1}.

3.2. Determination of water soluble mercury (Hg_{sl})

The mercury water soluble fraction in the soil was determined using the first step of the selective extractions proposed by Bloom *et al.*[20] and modified by using local rain water (Table 1). These data allow the quantity of available water soluble mercury concentrations in the samples to be determined, as it is known from previous studies that mercury associated with the soil aqueous phase is one of the key parameters affecting the MEF from soils.[29–32] Concentrations are at least two orders of magnitude below those of total mercury, and provide no evidence for a direct relationship with total Hg values. Variability at the LCM site is very low, with concentrations ranging from 2 to 150 ng g^{-1}, while in CMA concentrations range between 20 and more than 11 000 ng g^{-1}, with maximum values for samples located on, or in close proximity to, the furnaces.

The high standard deviation for the samples with higher mercury contents is due to the effect caused by the presence of mercury droplets and HgS particles acting as nuggets, for which reason it was difficult to achieve homogeneity of the samples analyzed.

3.3. Determination of mercury emission

(a) Effects of soil temperature. The total Hg concentration for LCM samples is not the main determining factor for the initial values when starting the volatilization of the element ($R^2 = 0.0036$, HgT *vs.* MEF) (Fig. 3A). This effect is probably related to the type of mercury species present in the soil, as observed by others (Lindberg *et al.*[33]). In particular, the sample showing the highest response to heat excitation (higher MEF) is W-28, taken from an allochthonous soil used to reclamate the mine dump, so the presence of mercury should be related to degassing processes from buried materials and to dry and wet deposition phenomena, due to its location (lee of the mine facilities). Likewise, the edaphic parameters determined in this sample are very favorable for mercury emissions, with slightly acid pH, low OM contents, poor in clay and low presence of salts. The lower reaction to temperature excitation in the rest of the samples could be

Table 1 Total mercury content and edaphic parameters for the different sampling sites

SP	W-30[a]	W-34[a]	W-28[a]	W-11[a]	W-10[a]	W-6[a]	W-15[a]	Al-2[b]	Al-24[b]	Alce-15[b]	Alce-13[b]	Alce-3[b]	Alce-8[b]	Alce-5[b]
Hg_T[c]	26 ± 9	185 ± 25	237 ± 57	415 ± 85	797 ± 29	1040 ± 21	1410 ± 75	75 ± 13	174 ± 20	736 ± 63	1880 ± 212	5500 ± 101	9770 ± 654	15 900 ± 1867
Hg_{sl}[d]	0.01 ± 0.01	0.01 ± 0.01	0.02 ± 0.01	0.01 ± 0.06	0.01 ± 0.05	0.10 ± 0.09	0.03 ± 0.01	0.03 ± 0.03	0.05 ± 0.04	0.02 ± 0.08	0.06 ± 0.03	4.270 ± 3.537	4.241 ± 2.051	11.362 ± 6.671
% OM[e]	4.3	1.9	1.2	1.5	2.2	4.1	3.7	2.7	3.8	4.6	5.9	3.8	2.2	1.7
pH[f]	5.0	5.9	6.2	5.0	5.7	6.0	6.2	8.0	8.4	8.0	7.7	8.1	8.0	8.6
EC[g]	185	344	73	81	167	373	227	182	322	298	325	214	318	182
% Clay	8	12	18	11	6	10	15	32	18	23	14	13	11	17
% Silt	13	12	13	14	7	15	11	12	10	18	12	12	9	15
% Sand	79	76	69	75	87	75	74	56	72	59	74	75	80	68
DES[h]	355	345	256	142	60	20	47	421	325	64	55	35	0	0

[a] W-samples correspond to the LCM area. [b] Al- and Alce-samples correspond to the CMA area. [c] (Total mercury) values in mg kg^{-1} ± standard deviation. [d] (Soluble mercury) values in mg kg^{-1} and ± standard deviation. [e] Percentage of organic matter. [f] Reactivity. [g] Electrical conductivity (μS cm^{-1}). [h] Distance to the emitting source in metres.

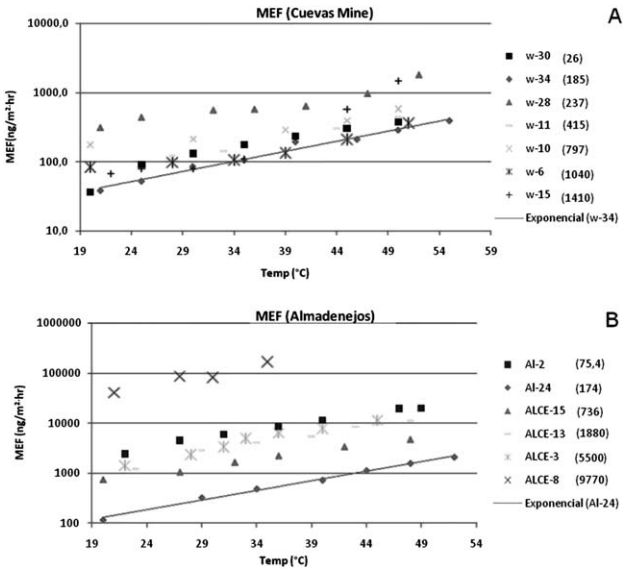

Fig. 3 Plot of mercury emission flux for soil samples from the Las Cuevas Mine (LCM) site (A) and CMA site (B). Total mercury content (mg kg^{-1}) for each sample is indicated in brackets to the left of the sample name.

explained by the presence of more stable Hg species, probably including cinnabar.

In contrast to the previous group, emission from the CMA samples (Fig. 3B) is directly governed by the soil total Hg contents ($R^2 = 0.7269$, HgT *vs.* MEF). However, sample Al-2 shows a higher response to excitation by temperature, emitting more mercury vapors than samples with higher contents of the element. This is due to the increment of the soluble mercury with higher total mercury contents. The samples with higher Hg contents (Alce-8 and Alce-5) tend to emit mercury vapor in larger quantities, even exceeding the equipment upper measurement range (20 000 ng m^{-3}).

One possible way to understand the processes driving thermally enhanced emission is to calculate the activation energy associated with the Hg flux. The activation energy (E_a) is the energy that the system needs to initiate an increase in the Hg flow.[34] It is assumed that the mercury species in the soil is Hg^0, which will be transferred to the atmosphere governed by a pseudo-first order reaction due to its temperature dependence of the Hg flux from the soil surface. The flow can be described by the Arrhenius equation (eqn (2)) by which the activation energy is calculated directly from the temperature dependence of MEF:[35]

$$\ln (\mathrm{MEF}) = \ln (A) - E_a/RT \quad (2)$$

where E_a is the apparent activation energy, A is the frequency factor, T the absolute temperature and R the gas constant. The concept of apparent activation energy refers to controlled thermal reactions.[35]

The activation energies calculated for our samples are in a good agreement with published data for mercury contaminated sites at which HgS is the predominant form of mercury.[36–38] Our results are also in good accordance with the Schlüter (2000)[1] proposal that the activation energy necessary for LCM samples shows a general tendency to decrease with increasing Hg concentration (Fig. 4A). It is, however, much higher for sample W-15, taken from the Las Cuevas mine entrance, and so presumably containing the highest cinnabar content. On the other hand, the sample W-28 shows a low E_a, and in turn has a higher mercury emission rate than samples with higher total mercury contents (Fig. 3A and Table 1). This anomaly clearly indicates the presence in this sample of a higher concentration of soluble mercury (Hg_{sl}), which is detected by the activation energy. On the other hand, at CMA the general tendency is that of higher E_a with larger total mercury contents (Fig. 4B). In this CMA sector a tendency is evident for higher values of E_a nearer to the emission sources (samples from metallurgical furnaces). This phenomenon is the result of the high amount of cinnabar in these samples, as well as the influence of alkaline pH, the presence of salts, and a considerable OM content. However, samples Al-2 and Alce-15 show a lower E_a which is reflected in the flux of mercury emissions for these samples (Fig. 4B). This effect is possible due to the breakdown of the structural characteristics of

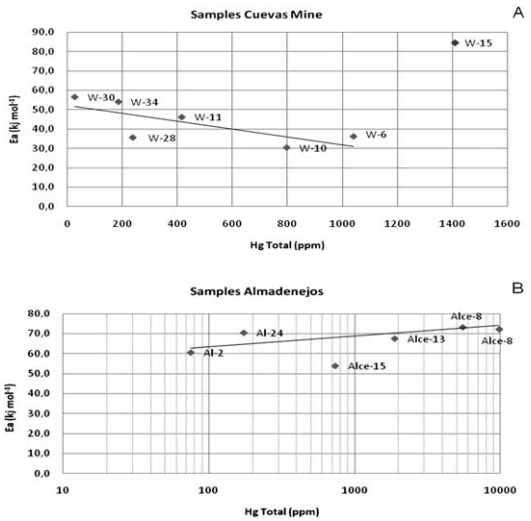

Fig. 4 Activation energies (E_a) for the LCM site (A) and CMA site (B). A trend line has been determined for the LCM site, excluding sample W-28, considered as an outlier (see text).

these samples with relatively high clay contents in relation with the temperature increase and sample drying.

(b) Effects of Hg fractionation in soil. Given the above considerations, quantification of Hg_{sl} is important in determining emission rates, since this Hg fraction is the one directly involved in soil volatilization.[37] Fig. 5 shows two highly contrasting scenarios: Las Cuevas (Fig. 5A) and Almadenejos (Fig. 5B). The values differ not only in orders of magnitude, but also in relative terms, that is, the distribution patterns are just so remarkably different.

In the CMA area (Table 1 and Fig. 5B), MEF is even more directly related to temperature and total mercury contents, due to the local direct relationship between total and soluble mercury. That is to say, the amount of soluble mercury increases with total mercury contents of these samples. In sample Al-2 specifically, the presence of Hg_{sl} and the textural characteristics of the soil (sandy clay loam) favor the processes of MEF, as well as a low content of organic matter and a low presence of the salts favors volatilization.

As noted above, the E_a can be used as a guide to infer the presence of labile Hg species in the soil—LCM samples (Fig. 6A) show a direct relationship between E_a and Hg_{sl}, although, for the CMA samples, this relationship is more tenuous (Fig. 6B). These differences should be clearly related to the fact that LCM is a mining area, in which most of mercury in the soil is in the form of cinnabar, while CMA is a metallurgical area, where the mercury species present in the soil are much more varied.[13]

(c) Effects of light radiation. The MEF experiments described above were carried out under room light conditions (*i.e.* dark conditions), considering only temperature variability. Here we describe and analyze the effects of higher light radiation on the samples, combined with the heating generated by the UV lamp.

The irradiation for all samples was carried out by means of a 32.6 klx ultraviolet lamp, 1 h approximately after verifying that MEF was stable in the initial conditions for the experiment

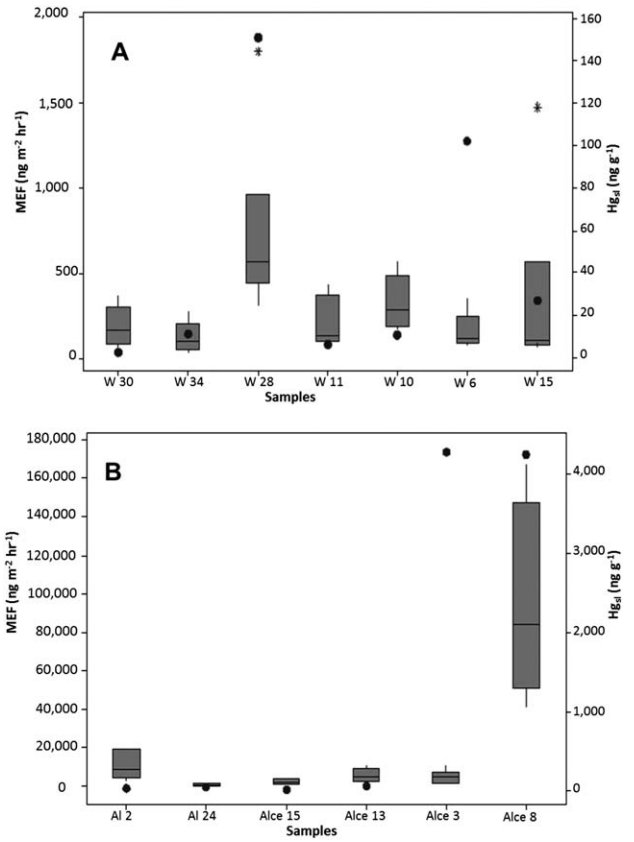

Fig. 5 Box and whisker plot of MEF, compared with that for Hg_{sl} for the same samples. (A) For the LCM site; and (B) for the CMA site.

(room temperature and radiation). The emission of all irradiated samples (Table 2 and Fig. 7A and B) was substantially greater than the MEF emission obtained under the dark conditions (Fig. 3A and B). As indicated, the observed temperature ramp corresponds to the effect of the UV lamp during the 40 to 120 min duration of each experiment (Table 2).

Additionally, and in the same way as in previous experiments, higher emission rates were observed from samples with

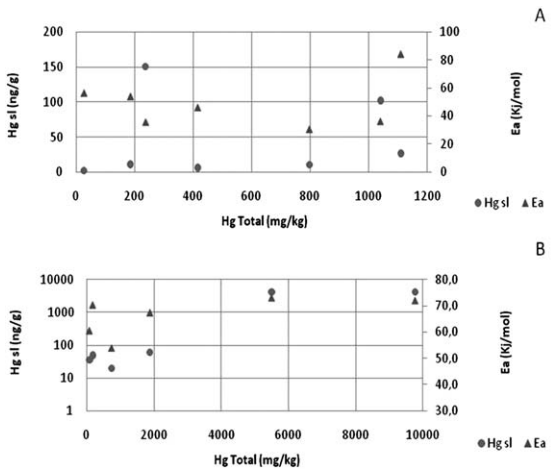

Fig. 6 Relations between activation energy (E_a) and soluble mercury (Hg_{sl}). (A) For the LCM site; and (B) for the CMA site.

Table 2 Comparison of mercury emissions with and without light radiation, and times required for maximum emissions and for emission decrease after UV light cessation

Sample	t_r [a]	t_{dr} [b]	MEF_{T° [c]	$MEF_{T^\circ+UV}$ [d]	T° [e]	T°_{UV} [f]
Al-2[g]	2.400	2.500	8.506	36.766	36	36
Alce-13[g]	3.100	10.300	5.457	12.123	39	39
Alce-15[g]	7.200	6.300	2.220	3.095	36	37
W-6[h]	6.300	4.500	135	1.126	39	37
W-10[h]	4.500	6.000	290	1.067	39	36
W-11[h]	4.500	6.000	142	465	34	37
W-28[h]	6.000	5.100	559	2.462	32	34

[a] Time needed for stabilization of mercury emission during the UV light emission (s). [b] Time needed for stabilization of mercury emission after cessation of the UV lighting (s). [c] Mercury emission flux for testing the temperature (ng m^{-2} h^{-1}). [d] Mercury emission flux for testing the temperature and radiation (ng m^{-2} h^{-1}). [e] Temperature emission under dark conditions (°C). [f] Temperature emission under radiation conditions (°C). [g] Samples correspond to the CMA area. [h] Samples correspond to the LCM area.

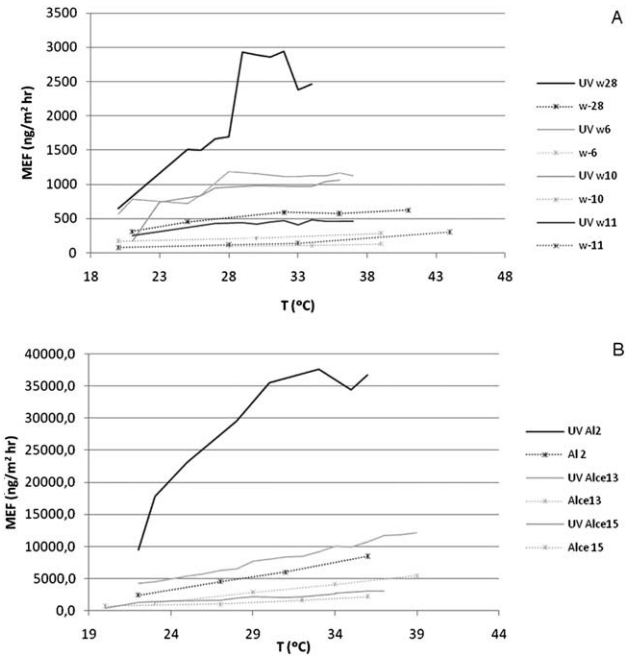

Fig. 7 Comparison of emission under light radiation (continuous solid lines) with emissions under dark conditions (dotted lines with asterisks) in LCM samples (A) and in CMA samples (B).

low total Hg but higher Hg_{sl} contents (Al-2 and W-28), while the rest of the samples have emission rates depending on the total mercury concentration. The values obtained reflect the importance of the role of light in the emission process, which is reflected in the 4-fold greater emission for Al-2 sample than that observed under dark conditions. It should also be noted that this sample is the one responding more quickly to light excitation (Table 2).

Additionally, we have analyzed the effect of abrupt cessation of light radiation (Fig. 8A and B), verifying that it produces a rapid adjustment of emission, reaching a stable baseline level determined by temperature, but with different stabilization times for each sample (Table 2).

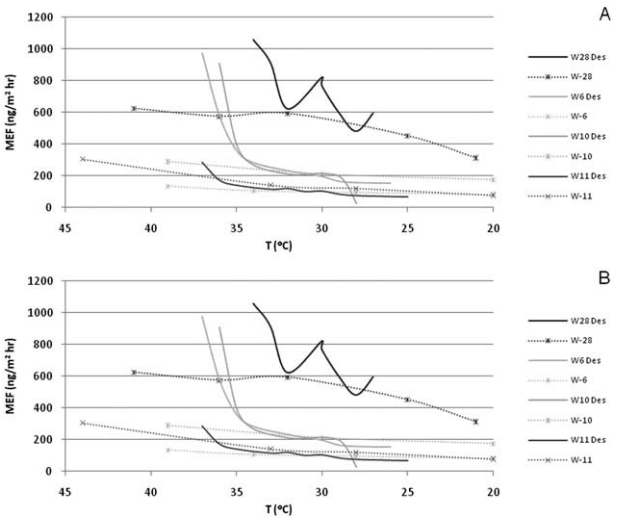

Fig. 8 Comparison of emissions after cessation of irradiation (continuous solid lines) with emission product of temperature (dotted lines with asterisks). (A) LCM site samples; and (B) CMA site samples.

3.4. Theoretical models of soil-related mercury concentration in the atmosphere

Following the above calculations for mercury emission, we carried out an integration of the different soil properties (total Hg concentration, Hg_{sl} content, MEF, soil texture, organic matter content, pH and conductivity) in order to identify areas of soil with characteristics similar to those producing emission values previously quantified in the laboratory. With the help of a Geographic Information System we have identified the areas of influence for emissions, which are used in the program ISC AERMOD to extend the point emission data to areal data. The software then performs the theoretical models for mercury concentration in air. Data used to implement the model were recorded exclusively in the year 2009 and in the CMA area, and we have used only the maximum temperatures reached by the soil in the different seasons (summer, spring, fall), corresponding to the moments of highest emission. In addition, we have used a database of atmospheric mercury concentrations, measured during several field surveys carried out in 2009 with a portable mercury analyzer (Lumex RA915+). These surveys were based in a unique regular-equidistant grid used in previous works.[14] To confirm the theoretical model we compared it with the field measurements. The resulting models and the isovalue maps obtained by means of kriging-based interpolation are displayed in Fig. 9. Similarities between the models and the real data based maps are evident, identifying how the area of higher concentration of atmospheric mercury corresponds to the metallurgical precinct. The theoretical model is able to characterize correctly the variations observed for the different seasons, calculating the largest plume dimensions for the periods of higher temperatures, and taking into account other variables, such as wind speed, which increases the plume size for the fall season, due to the effects of dilution and transport speed. In both theoretical and experimental cases there is an evident transport of pollution southward, affecting the Almadenejos urban area, with values that could be of concern, especially during summertime.

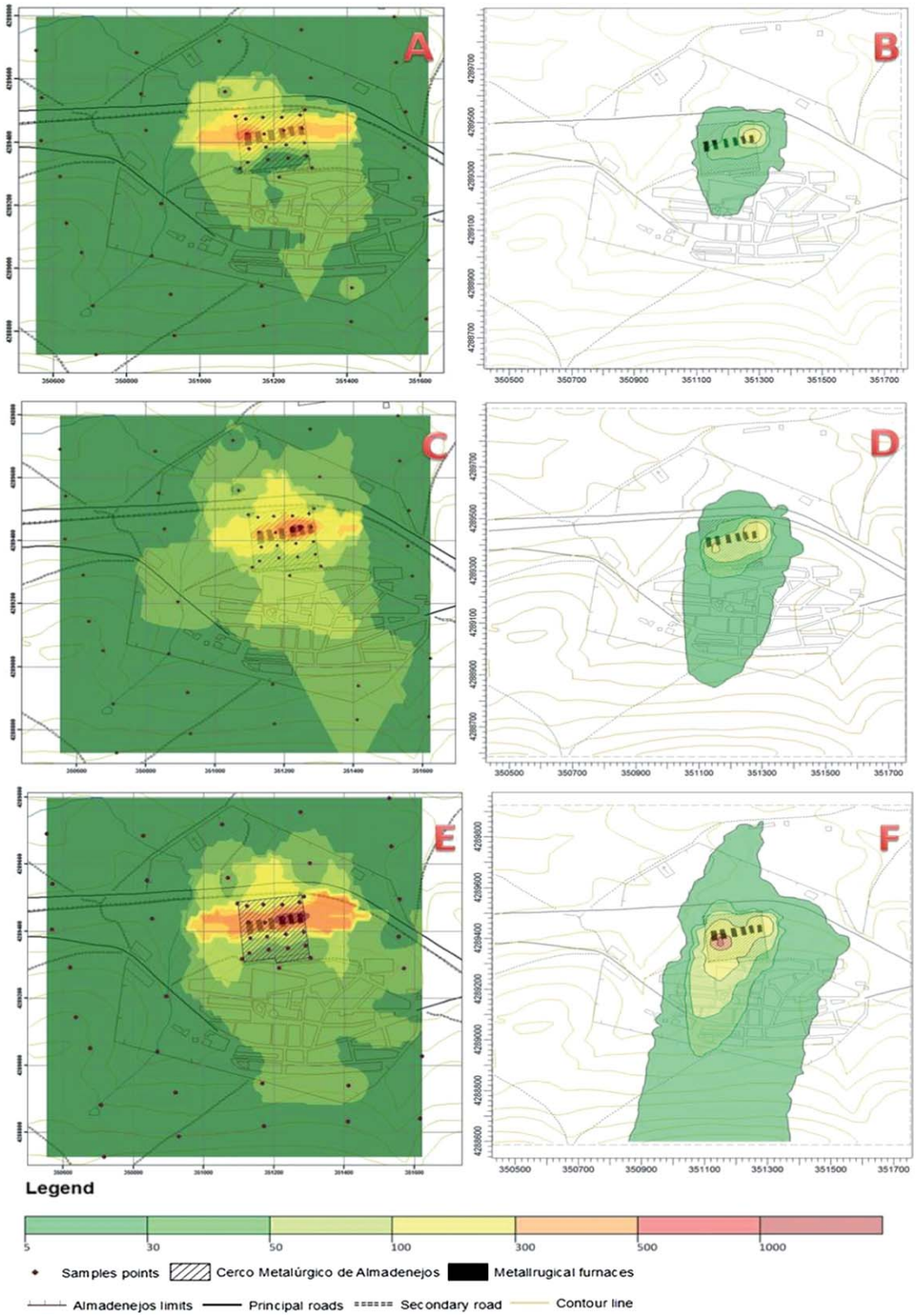

Fig. 9 Theoretical models (A, C and E) and experimental data (B, D and F) for atmospheric mercury concentrations during fall (A and B), spring (C and D) and summer (E and F). All values in ng m^{-3}.

The estimation of mercury emission for the CMA area for the complete year 2009 is: 7.26 kg y^{-1} (summer), 5.59 kg y^{-1} (spring), 2.58 kg y^{-1} (fall) and 1.0 kg y^{-1} (winter), totalling 16.43 kg y^{-1}. This is similar to non-point source Hg releases recently reported for Cortez-Pipeline gold mine in Nevada.[39] This emission is calculated just on the basis of excitation temperature, not

considering the radiation effects. Similarly these calculations were performed using the following soil temperatures for each season: 35 °C (summer), 27 °C (spring), 24 °C (fall), and 20 °C (winter).

4. Conclusions

This study was aimed at determining the main parameters involved in the emission of mercury vapour from heavily contaminated soils in two areas, one affected by mining activity (LCM area) and the other by metallurgical activity (CMA area). Analysis of the results indicates that the factors to highlight are temperature, light radiation and the concentration of soluble mercury in soils.

The results for total Hg and Hg_{sl} indicate that insoluble species, more than likely cinnabar, are the major mercury components of the soils studied, with notable differences between the two areas, pointing out that CMA is richer in soluble species. These results are in good agreement with the activation energies calculated for the emission process at the two sample locations.

In the same way, mercury emission is more rapid and intense in the areas with soluble forms of mercury (CMA) than in those with insoluble forms (LCM). These results indicate the usefulness of simple fractionation using the water soluble fraction of mercury in soil to estimate the potential for mercury emission from contaminated land.

Data from the earlier part of this study have been applied to characterizing the gaseous mercury plume generated by soil-originated emissions in different seasons, It has been shown that higher emission and larger plume size are generated in dry and warm periods (summer), while the plume is smaller and involves lower concentrations of atmospheric mercury during colder periods with higher wind activity, such as fall. The orientation of pollutant plumes (North–South) is very similar in the two types of models.

On the basis of our emission calculations and the model implementation for the CMA metallurgical precinct (Cerco Metalúrgico de Almadenejos), annual emissions for this area are estimated to be 16.4 kg Hg y^{-1}, with important differences between hot and cold seasons.

Acknowledgements

This work has been funded by Spanish Ministry of Science and Innovation (MICINN), through the Projects CTM2006-13091-C02-01/TECNO and CGL2009-13171-C03/BTE. WL is granted by the "Becas de Formación de Personal Investigador"/ MICINN (BES-2007-16807) program, and his stay at the Jožef Stefan Institute (Ljubljana) was funded by grant SES-T1000I000985XV0/MICINN. The work at the JSI was funded through the ARRS programme P1-0143.

References

1 K. Schlüter, *Environ. Geol.*, 2000, **39**, 249–271.
2 E. Pacyna, J. Pacyna, K. Sundseth, J. Munthe, K. Kindbom, S. Wilson, F. Steenhuisen and P. Maxson, *Atmos. Environ.*, 2010, **4**, 2487–2499.
3 N. Pirrone, S. Cinnirella, X. Feng, R. B. Finkelman, H. R. Friedli, J. Leaner, R. Mason, A. B. Mukherjee, G. Stracher, D. G. Streets and K. Telmer, *Atmos. Chem. Phys.*, 2010, **10**, 5951–5964.
4 M. S. Gustin, *Sci. Total Environ.*, 2003, **304**, 153–167.
5 M. S. Gustin, G. E. Taylor Jr. and R. A. Maxey, *J. Geophys. Res.*, 1997, **102**, 3891–3898.
6 M. Coolbaugh, M. Gustin and J. Rytuba, *Environ. Geol.*, 2002, **42**, 338–349.
7 S. Wang, X. Feng, G. Qiu, Z. Wei and T. Xiao, *Atmos. Environ.*, 2005, **39**, 7459–7473.
8 D. Kocman and M. Horvat, *J. Environ. Manag.*, 2011, **92**(8), 2038–2046.
9 S. Lindberg, R. Bullock, R. Ebinghaus, D. Engstrom, X. Feng, W. Fitzgerald, N. Pirrone, E. Prestbo and C. Seigneur, *Ambio*, 2007, **36**, 19–33.
10 A. Hernández, M. Jébrak, P. Higueras, R. Oyarzun, D. Morata and J. Munhá, *Miner. Deposita*, 1999, **34**, 539–548.
11 P. Higueras, R. Oyarzun, H. Biester, J. Lillo and S. Lorenzo, *J. Geochem. Explor.*, 2003, **80**, 95–104.
12 P. Higueras, R. Oyarzun, J. Lillo, J. C. Sánchez-Hernández, J. A. Molina, J. M. Esbrí and S. Lorenzo, *Sci. Total Environ.*, 2006, **356**, 112–124.
13 J. E. Gray, M. E. Hines, P. L. Higueras, I. Adatto and B. K. Lasorsa, *Environ. Sci. Technol.*, 2004, **38**(16), 4285–4292.
14 A. Martínez-Coronado, R. Oyarzun, J. M. Esbrí, W. Llanos and P. Higueras, *J. Geochem. Explor.*, 2011, **109**, 70–77.
15 P. Higueras, R. Oyarzun, R. Lunar, J. Sierra and J. Parras, *Miner. Deposita*, 1999, **34**(2), 211–214.
16 W. Llanos, P. Higueras, R. Oyarzun, J. M. Esbrí, M. A. López-Berdonces, E. M. García-Noguero and A. Martínez-Coronado, *Sci. Total Environ.*, 2010, **408**, 4901–4905.
17 A. Walkley and I. Black, *Soil Sci.*, 1934, **37**, 29–38.
18 L. E. Allison, *J. Am. Soc. Agron.*, 1965, **9**, 1367–1378.
19 S. Sholupov, S. Pogarev, V. Ryzhov, N. Mashyanov and A. Stroganov, *Fuel Process. Technol.*, 2004, **85**, 473–485.
20 N. S. Bloom, E. Preus, J. Katon and M. Hiltner, *Anal. Chim. Acta*, 2003, **479**, 233–248.
21 W. H. Schroeder and J. Munthe, *Atmos. Environ.*, 1998, **32**, 809–822.
22 Z. F. Xiao, J. Munthe, W. H. Schroeder and O. Lindqvist, *Tellus, Ser. B*, 1991, **43**, 267–279.
23 K.-H. Kim and S. E. Lindberg, *Atmos. Environ.*, 1995, **29**(2), 267–282.
24 R. Ferrara and B. A. Mazzolai, *Sci. Total Environ.*, 1998, **215**, 51–57.
25 R. Ferrara, B. Mazzolai, E. Lanzillotta, E. Nucaro and N. Pirrone, *Sci. Total Environ.*, 2000, **259**, 183–190.
26 L. Poissant and A. Casimir, *Atmos. Environ.*, 1998, **32**, 883–893.
27 D. Y. Jing, Z. L. He and X. E. Yang, *Chemosphere*, 2007, **69**, 1662–1669.
28 D. Wallschläger, M. V. M. Desai, M. Spengler and R. D. Wilken, *J. Environ. Qual.*, 1998, **27**, 1044–1054.
29 M. Xin, M. Gustin and D. Johnson, *Environ. Sci. Technol.*, 2007, **41**, 4946–4951.
30 A. Carpi and S. E. Lindberg, *Environ. Sci. Technol.*, 1997, **31**, 2085–2091.
31 A. Carpi and S. E. Lindberg, *Atmos. Environ.*, 1998, **32**, 873–882.
32 A. Gillis and D. R. Miller, *Sci. Total Environ.*, 2000, **260**, 191–200.
33 S. E. Lindberg, H. Zhang, M. S. Gustin, A. Vette, F. Marsik, J. Owens, A. Casimir, R. Ebinghaus, G. Edwards, C. Fitzgerald, J. Kemp, H. H. Kock, J. London, M. Majewski, L. Poissant, P. Pilote, P. Rasmussen, F. Schaedlich, D. Schneeberger, J. Sommar, R. Turner, D. Wallschläger and Z. Xiao, *J. Geophys. Res.*, 1999, **104**, 21879–21888.
34 S. Gustin, M. Coolbaugh, M. Engle, J. Fitzgerald, C. Sladek, H. Zhang and R. Zehner, *Environ. Geol.*, 2003, **43**, 339–351.
35 E. Bahlmann, R. Ebinghaus and W. Ruck, *J. Environ. Manage.*, 2006, **81**, 114–125.
36 S. E. Lindberg, K.-H. Kim, T. P. Meyers and J. G. Owens, *Environ. Sci. Technol.*, 1995, **29**, 126–135.
37 D. Kocman and M. Horvat, *Atmos. Chem. Phys.*, 2010, **10**, 1417–1426.
38 M. S. Gustin, J. R. Taylor and R. A. Maxcy, *J. Geophys. Res.*, 1997, **102**, 3891–3898.
39 C. S. Eckley, M. Gustin, M. B. Miller and F. Marsik, *Environ. Sci. Technol.*, 2011, **45**, 392–399.

